JACS
JOURNAL OF THE AMERICAN CHEMICAL SOCIETY
Article
pubs.acs.org/JACS

On the Nature of Ge−Pb Bonding in the Solid State. Synthesis, Structural Characterization, and Electronic Structures of Two Unprecedented Germanide-Plumbides

Nian-Tzu Suen,[†] James Hooper,[‡] Eva Zurek,*[,‡] and Svilen Bobev*[,†]

[†]Department of Chemistry and Biochemistry, University of Delaware, Newark, Delaware 19716, United States
[‡]Department of Chemistry, University of Buffalo, Buffalo, New York 14260, United States

Supporting Information

ABSTRACT: Reported are the syntheses and the crystallographic characterization of two structurally related solid-state compounds: $(Eu_{1-x}Ca_x)_2Ge_2Pb$ (space group *Pbam*) and $(Sr_xEu_{1-x})_2Ge_2Pb$ (space group *Cmmm*). Both structures boast anionic sublattices with fully ordered Ge and Pb at the atomic level, which is unusual for elements of the same group. Despite the nearly identical formulas and the similar chemical makeup, the nature of the chemical bonding in the two compounds is subtly different; in the $(Eu_{1-x}Ca_x)_2Ge_2Pb$ structure, Ge and Pb are positioned at a relatively shorter distance from one another (<3.0 Å). The close proximity of the atoms leads to interactions, which are seen for the first time in an extended structure and can be suggested to have a covalent character. This conjecture is supported by extensive electronic band-structure calculations using first principles. Magnetic susceptibility measurements reveal Eu^{2+} ground state ($[Xe]4f^7$ configuration) and the presence of an antiferromagnetic ordering at cryogenic temperatures.

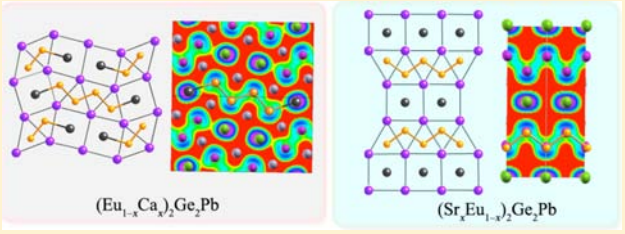

1. INTRODUCTION

During the past 3−4 decades, studies of a variety of polar intermetallic compounds have shown an enormous diversity of structures and a wealth of unusual physical properties.[1−10] In most simplistic terms, the chemical bonding in such compounds can be regarded as bridging the typical Zintl phases and the typical intermetallic compounds.[3−6] For example, focusing our attention on a relatively small subset of materials, the rare-earth metal germanides, our group has shown that the formally reduced germanium atoms can assemble into many kinds of (poly)anions, such as Ge_2 dimers in Ln_2MgGe_2,[11] and $Ln_3Li_4Ge_4$[12] (Ln = lanthanide element or rare-earth metal, used interchangeably hereafter), one-dimensional zigzag chains in $LnLiGe_2$,[13] cis−trans chains in $Ln_2Li_2Ge_3$,[12] flat or puckered two-dimensional layers in Ln_3Ge_5,[14] and $EuGe_2$,[15] respectively.

Regardless of the large differences in the crystal chemistry, many of the above-mentioned bonding patterns can be understood as combinations of simpler structures (Figure 1), "colored"[16] according to the atomic sizes and the number of valence electrons; after all, these are the two main factors that determine the bonding in similar metallic systems. However, as the structural complexity increases, and the electronegativity/size differences diminish, the energy difference between various atomic arrangements becomes diminutive.[17] Of specific relevance here is the question how do elements from the same group arrange themselves within an extended structure; that is, how do the unchanged electronic requirements (neglecting the relativistic effects) affect the packing of atoms with very different atomic radii and slightly different electronegativities? In this Article, we offer new insights into these outstanding issues with regard to Ge and Pb, by detailing the structures of the two novel germanide-plumbides, $Eu_{1.32}Ca_{0.68(1)}Ge_2Pb$ (compound **I**) and $Sr_{0.42}Eu_{1.58(2)}Ge_2Pb$ (compound **II**). Their structures are similar to each other and can be recognized as 1:1 intergrowths of CsCl- and AlB_2-like fragments,[18] yet in a different fashion, which provided us good examples to study the interactions between these elements. Therefore, the nature of the bonding of these two compounds was interrogated in depth using first-principles calculations based on plane-waves and pseudopotentials, as well as tight-binding calculations. Via analyses of the electronic densities of states, electron localization functions, Bader charges, as well as the crystal orbital Hamilton populations, it was illustrated that a full donation of charge from the cationic to the anionic sublattices does not occur, and signatures of covalent bonding between Ge and Pb were observed in compound **I**.

2. EXPERIMENTAL SECTION

2.1. Synthesis. All starting materials were purchased from common chemical vendors (Alfa, Aldrich) and used as received (in an argon-filled glovebox). The title compounds can be synthesized by either flux reactions[18] (lead flux) or by loading the corresponding elements in stoichiometric ratios in niobium containers. Below, we describe the flux reactions as the most successful route toward the title compounds.

Received: May 5, 2012
Published: July 6, 2012

   dx.doi.org/10.1021/ja3042838 | *J. Am. Chem. Soc.* 2012, 134, 12708−12716

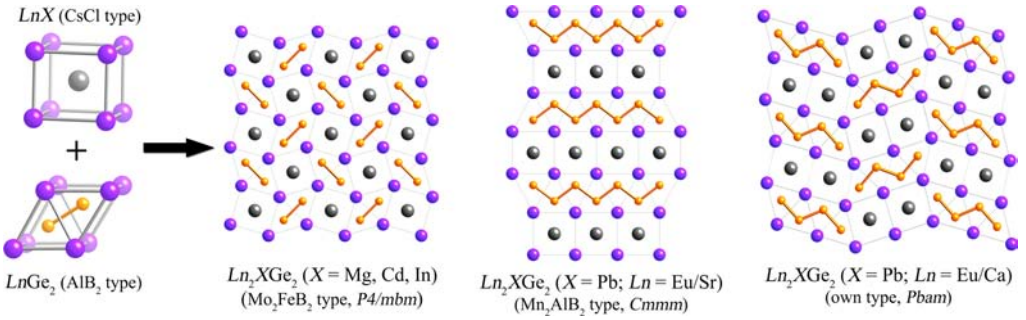

Figure 1. Three different structures, which can be visualized as 1:1 intergrowths of CsCl- and AlB_2-like motifs, are depicted. The diverse Ge (poly)anions are emphasized. There are Ge_2 dumbbells in Ln_2XGe_2 (Ln = lanthanide element; X = Mg, Cd, In); infinite $[Ge_2]$ zigzag chains in $(Sr_xEu_{1-x})_2Ge_2Pb$; and *trans*-butene-like $[Ge_4]$ fragments in $(Eu_{1-x}Ca_x)_2Ge_2Pb$.

$(Eu_{1-x}Ca_x)_2Ge_2Pb$ (x = 0.34(1)) was first obtained from a Pb-flux reaction loaded as 3:2:3:6 (Eu:Ca:Ge:Pb). The elements were loaded in an alumina crucible and subsequently enclosed in an evacuated (ca. 10^{-3} Torr) silica jacket by flame sealing. The silica ampules were then heated to 800 °C at a rate of 200 °C/h and homogenized for 24 h. After that, the temperature was slowly lowered to 600 °C (5 °C/h), and the ampules were taken out, inverted, and spun off with a centrifuge to remove the excess molten Pb. After the as-synthesized product was checked via powder and single-crystal X-ray diffraction, the following phases in nearly equal yields were identified: (1) $CaPb_3$[19] (silver cube-like shape); (2) $(Eu_{1-x}Ca_x)_2Ge_2Pb$ (black shiny rod-like shape); and (3) EuGe (black shiny plate-like shape).[13] A small amount of leftover elemental germanium (silver irregular) was also detected. Avoiding the formation of $CaPb_3$ was a challenge and a critical element of the synthetic work; it appeared that once this phase has formed, the nominal composition changes, and, as a result, both EuGe[13] and $EuGe_2$[15] also precipitate. By trial and error experiments, we found that lowering the amount of lead helped decrease the amount of $CaPb_3$; however, too little lead will also cause greater inhomogeneity in the product. The best way we found to maximize the yield of compound **I** was to carry out the synthesis with the ratio 3:2:3:4 (Eu:Ca:Ge:Pb) at 800 °C (5 h) and remove at temperature above the melting point of $CaPb_3$ (mp 660 °C).[20] To remove the traces of residual Pb/$CaPb_3$, the raw product was washed by a mixed solution of equal volumes H_2O_2 (3%) and acetic acid (1 M). Following this synthetic route, we were able to obtain compound **I** with sample purity up to 95%. $(Sr_xEu_{1-x})_2Ge_2Pb$ (x = 0.21(1)) was synthesized using the same procedure. Some of the crystals were up to 1 mm × 1 mm × 5 mm in size.

We must also note that despite the many different experimental conditions we tried (different loading ratios or different heating profiles), the ternary compounds Eu_2Ge_2Pb, Ca_2Ge_2Pb, and Sr_2Ge_2Pb were never obtained. It appears that the new phases are true quaternaries and only form with mixed Eu/Ca or Sr/Eu. While we did not conduct a full study on the stoichiometry breadths of compounds **I** and **II**, on the basis of the results from all experiments we can speculate that they form only in fairly narrow compositional ranges. For example, the structural discussion in the main text is based on the $Eu_{1.32}Ca_{0.68(1)}Ge_2Pb$ crystal structure (Table 1, unit cell volume 532.3(3) Å^3); however, we have collected multiple data sets for crystals from different batches and have found that the Ca fraction can be decreased from 30% to 15% ($Eu_{1.69}Ca_{0.31(1)}Ge_2Pb$ with cell volume 543.0(2) Å^3; see Table S1 in the Supporting Information).

We also tried Eu/Yb and Ba/Eu mixtures to extend this chemistry, but so far found only evidence for the existence of the latter. Interestingly, for the Ba-analogue, it appeared that it could adopt both structures and the structure control is achieved by changing the loading ratio of the elements. For example, when the ratio Ba:Eu:Pb:Ge = 2:3:4:3 was used, the reaction afforded $(Ba_xEu_{1-x})_2Ge_2Pb$ with the *Cmmm* structure. Conversely, the Ba-leaner reaction mixture (Ba:Eu:Pb:Ge = 1:3:4:3 Eu:Ba:Pb:Ge) afforded as major product the phase with the *Cmmm* structure and minor phase with the *Pbam* structure. This work is currently ongoing, and more experimental details concerning these two structures will be presented in a forthcoming paper.

Table 1. Selected Single-Crystal Data Collection and Refinement Parameters for Compounds I and II

empirical formula	$Eu_{1.32}Ca_{0.68(1)}Ge_2Pb$	$Sr_{0.42}Eu_{1.58(2)}Ge_2Pb$
formula weight	630.23, Z = 4	580.77, Z = 2
radiation	Mo Kα, 0.71073 Å	
temperature	200 K	
space group	*Pbam* (No. 55)	*Cmmm* (No. 65)
unit cell dimensions, Å	a = 7.875(3)	a = 3.9890(14)
	b = 14.873(5)	b = 15.243(5)
	c = 4.5444(15)	c = 4.5365(16)
unit cell volume, Å^3	532.3(3)	275.84(17)
ρ_{calc}, g cm^{-3}	7.237	7.588
absorption coeff., cm^{-1}	585.67	627.67
GOF on F^2	1.034	1.184
data/parameters	600/34	183/13
R_1 ($I > 2\sigma_{(I)}$)[a]	0.0182	0.0279
wR_2 ($I > 2\sigma_{(I)}$)[a]	0.0378	0.0601

[a] $R_1 = \sum||F_o| - |F_c||/\sum|F_o|$; $wR_2 = [\sum[w(F_o^2 - F_c^2)^2]/\sum[w(F_o^2)^2]]^{1/2}$, and $w = 1/[\sigma^2F_o^2 + (A\cdot P)^2 + B\cdot P]$, $P = (F_o^2 + 2F_c^2)/3$; A and B are weight coefficients.

2.2. Structure Determination. X-ray powder diffraction patterns were collected at room temperature on a Rigaku MiniFlex diffractometer (filtered Cu Kα radiation). The data collection was in the 15−65° 2θ range with scan-mode 0.05°/step and 10 s/step counting time. Data analysis was done using the JADE 6.5 software package. The positions and the intensities of the Bragg peaks matched the calculations from the refined structures. Samples prepared for magnetic susceptibility measurements were also checked to ensure purity. On the basis of their powder diffraction patterns, both compounds were determined to be stable on a laboratory bench at least for 1 month.

X-ray single-crystal diffraction data were acquired on a Bruker SMART CCD-based diffractometer (monochromatized Mo Kα radiation, λ = 0.71073 Å). Crystals of the title compounds were cut under an optical microscope and mounted on glass fibers with Paratone-N oil. The crystals were cooled to 200 K through evaporating liquid nitrogen, and preliminary rotation images were acquired to assess the crystal quality. Full spheres of reciprocal data with frame width 0.3° were gathered. Data acquisition and integration were done using the programs SMART and SAINTplus,[21] respectively. Semi-empirical absorption correction was applied using SADABS.[22] The structures were refined by full-matrix least-squares methods (on F^2), as implemented in SHELXTL.[23] Refined parameters included the scale factor, extinction coefficients, and atomic positions with the corresponding anisotropic displacement parameters (Table 1). The occupation factors of the Eu/Ca and Sr/Eu positions were also refined,

dx.doi.org/10.1021/ja3042838 | J. Am. Chem. Soc. 2012, 134, 12708−12716

and the obtained compositions were in excellent agreement with the results from the elemental microanalysis (vide infra).

The atomic positions were standardized by STRUCTURE TIDY.[24] Final atomic coordinates and equivalent isotropic displacement parameters are given in Tables 2 and 3, respectively. Selected interatomic distances are tabulated in Table 4.[25]

2.3. Elemental Analysis. Several crystals from different batches were picked and washed by mixed solution (H_2O_2 and acetic acid) and then mounted on conductive carbon tape. The compositions of these crystals were analyzed with a JEOL 7400F electron microscope equipped with an INCA-OXFORD energy-dispersive spectrometer (EDS). The beam current was 10 μA at 15 kV accelerating potential, and the counting time for each spot was 120 s.

2.4. Magnetic Susceptibility Measurements. Temperature-dependent DC magnetization measurements were performed within the range from 5 to 300 K and an applied field of 5000 Oe. The data were acquired in a PPMS (Quantum Design) system for two batches from each phase to ensure reproducibility. The raw data were corrected for the holder contribution and converted to molar magnetic susceptibility ($\chi = M/H$).

2.5. Computational Details. First principles DFT calculations were performed with the Vienna ab initio Simulation Package (VASP) version 4.6.31.[26] The projector augmented wave (PAW) method[27] was used to treat the core states, and a plane-wave basis set with an energy cutoff of 500 eV was employed. The Pb 6s/6p, Ge 4s/4p, Ca 3p/4s, Sr 4p/5s, and Eu 5p/6s electrons were treated explicitly in all of the calculations presented in the main text. The results were compared to those obtained when the Eu $5d^14f^6$ states were treated explicitly, and it was confirmed that the projected densities of states for Pb and Ge were relatively independent from the choice of pseudopotential used for Eu. The gradient-corrected exchange and correlation functional of Perdew–Burke–Ernzerhof (PBE)[28] was adopted, and the *k*-point grids were generated using the Γ-centered Monkhorst–Pack scheme. The number of divisions along each reciprocal lattice vector was chosen such that the product of this number with the real lattice constant was 50 Å. The calculations on the $[Pb_2Ge_4]^{q-}$ molecular fragments and $(p\text{-}Tol)_3PbGePh_3$[29] were performed using the ADF molecular program,[30] the PBE functional, and a TZP basis set from the ADF basis set library. The Pb 5d/6s/6p and Ge 3d/4s/4p and C 2s/2p electrons were treated as valence in the ADF calculations. Scalar relativistic effects[31] were included in the results presented in the main text, and it was found that spin–orbit coupling did not influence the electronic structure noticeably (other than the slight splitting of degenerate states).

To supplement the VASP calculations, the band structures, densities of states (DOS), and crystal orbital Hamilton populations (COHP)[32] curves of structural models for compounds **I** and **II**, $EuCaGe_2Pb$ and $SrEuGe_2Pb$, were calculated using the tight-binding linear muffin-tin orbital (TB–LMTO) method[33,34] in the atomic-sphere approximation (ASA). The VWN[35] local exchange correlation potential was used along with the Perdew–Wang[36] generalized gradient approximation. The basis consisted of s, p, and d functions for Ca, Sr, Ge, Pb, and Eu. Scalar relativistic effects were included. No empty interstitial spheres were inserted, with the maximum sphere overlap being 16%. The calculations utilized 1729 and 1197 irreducible points in the tetrahedron *k*-space integrations[37] to calculate the DOS plots of structures **I** and **II**, respectively. The TB-LMTO DOS and ELF plots showed good agreement with those obtained with VASP. The band structures decorated with orthonormal LMTO characters, wherein the band-widths are proportional to a particular orbital character (fat bands), are also provided.

3. RESULTS AND DISCUSSION

3.1. Structure Description and Chemical Bonding. The following paragraphs detail the results from the structural characterization and the electronic structure calculations of two related compounds: $Eu_{1.32}Ca_{0.68(1)}Ge_2Pb$ and $Sr_{0.42}Eu_{1.58(2)}Ge_2Pb$. Their structures are indeed very similar to one another, and both can be recognized as 1:1 intergrowths of CsCl- and AlB_2-like fragments (Figure 1). As seen from the figure, intergrowths of the above two structures are not uncommon; Ln_2XGe_2 (X = Mg, Cd, In), among others, can also be viewed as combinations of the same building blocks.[38] The difference between these three structures is in the way the CsCl- and AlB_2-like substructures are interconnected. This results in bonding environments of the Ge atoms, which constitute the major structural distinction; there are $[Ge_2]$ dimers in Ln_2XGe_2, tetrameric $[Ge_4]$ fragments in compound **I**, and infinite $[Ge_2]$ zigzag chains in compound **II**, respectively. Therefore, interrogating the structures at greater depth is also warranted here, and, in particular, pointing out the subtle nuances in the Ge–Ge bonds.

Table 2. Atomic Coordinates and Equivalent Isotropic Displacement Parameters (U_{eq}[a]) for Compound I

atom	Wyckoff	*x*	*y*	*z*	U_{eq} [Å]^2
M1[b]	4*g*	0.1047(1)	0.2799(1)	0	0.014(1)
M2[b]	4*g*	0.2497(1)	0.0357(1)	0	0.014(1)
Ge1	4*h*	0.0586(1)	0.4221(1)	1/2	0.015(1)
Ge2	4*h*	0.3167(1)	0.1892(1)	1/2	0.012(1)
Pb1	4*h*	0.4369(1)	0.3757(1)	1/2	0.016(1)

[a]U_{eq} is defined as one-third of the trace of the orthogonalized U_{ij} tensor. [b]The final refined Eu/Ca occupancies are Eu/Ca = 0.512/0.488(3) for M1; Eu/Ca = 0.812/0.188(3) for M2.

Compound **I** crystallizes in a new structure type[39] with the orthorhombic space group *Pbam* (No. 55, $Z = 4$) and has a Pearson symbol *oP*16.[19] There are five crystallographically unique atoms in the asymmetric unit: two alkaline-earth/rare-earth metal, two Ge, and one Pb atoms (Table 2).

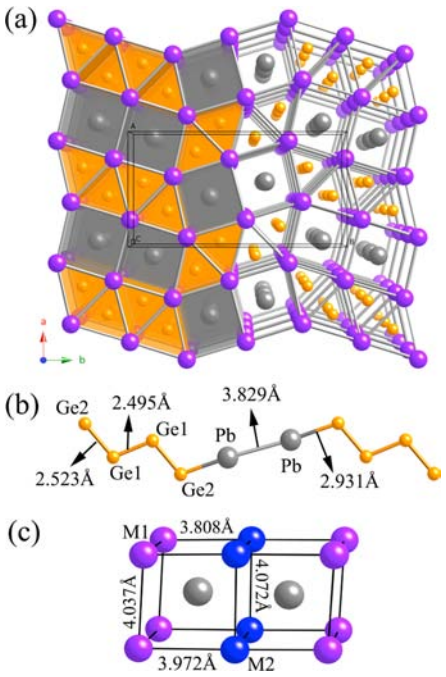

Figure 2. (a) Perspective view of the crystal structure of compound **I**. CsCl- and AlB_2-like building blocks are emphasized. (b) The *trans*-butene-like $[Ge_4]$ fragments, linked via Pb atoms. (c) The 8-fold (distorted-cubic) coordination of the Pb atoms (M1 and M2 are mixed-occupied Eu and Ca; see Table 2).

dx.doi.org/10.1021/ja3042838 | J. Am. Chem. Soc. 2012, 134, 12708–12716

The *trans*-butene-like [Ge_4] anion is the hallmark of this bonding arrangement (Figure 2). There are two types of Ge−Ge bonds: $d_{Ge1-Ge1}$ = 2.495(2) Å and $d_{Ge1-Ge2}$ = 2.523(1) Å. On the basis of that, one could argue that there is partial double-bond character of the Ge1−Ge1 interactions, while the Ge1−Ge2 ones resemble more closely the single 2-center-2-electron bonds. The Ge−Ge distances match well with those in other alkaline-earth or rare-earth metal germanides (d_{Ge-Ge} = 2.541(1) Å in $CaGe_2$,[40] d_{Ge-Ge} = 2.564(1) Å in $EuGe_2$,[15] d_{Ge-Ge} = 2.506(2)−2.548(1) Å in Ln_2MgGe_2,[11] d_{Ge-Ge} = 2.522(1) Å in EuInGe,[41] among others). One may recall that $(Eu_{1-x}Ca_x)_2Ge_2Pb$ has a small stoichiometry breadth, concomitant with the 2−3% change in the unit cell volume as the Eu/Ca ratios are varied. Notably, the shortest Ge−Ge distances are invariant of these changes, while the longer Ge−Ge and Ge−Pb distances increase slightly (see Table S3 in the Supporting Information).

Notice also the Pb−Ge2 contact (d_{Pb-Ge2} = 2.931(2) Å), slightly longer than the sum of the Pauling's covalent radii (r_{Ge} = 1.242 Å; r_{Pb} = 1.502 Å),[42] yet appreciably shorter than the 3.065(2) Å distance in compound **II** (vide infra). $(p\text{-}Tol)_3PbGePh_3$ is a molecular example with covalent Pb−Ge bonding,[29] where the distance is 2.642(1) Å (the first of only four crystallographically characterized molecules in CCDC). From the discussed structural parameters, it can be concluded that some degree of covalency in the Pb−Ge interaction should be expected. This point is critical to understanding the electron count and is further developed in the discussion of the electronic structure.

Compound **II** crystallizes in orthorhombic space group *Cmmm* (No. 65, Z = 2), and it is isotypic to Mn_2AlB_2,[43] which has Pearson symbol *o*C10.[19] There are three crystallographically unique atoms in the asymmetric unit (Table 3).

Table 3. Atomic Coordinates and Equivalent Isotropic Displacement Parameters (U_{eq}[a]) for Compound II

atom	Wyckoff	x	y	z	U_{eq} [Å]^2
M1[b]	4*j*	0	0.3697(1)	1/2	0.012(1)
Ge1	4*i*	0	0.2011(1)	0	0.013(1)
Pb1	2*a*	0	0	0	0.015(1)

[a] U_{eq} is defined as one-third of the trace of the orthogonalized U_{ij} tensor. [b] The final refined Sr/Eu occupancy at the M1 site is 0.202/0.798(8).

The most prominent feature in this structure (Figure 3) is the one-dimensional $^1_\infty$[Ge_2] chain, which is also found in many other binary or ternary compounds such as EuGe (CrB structure type) and $EuLiGe_2$ ($CaLiSi_2$ structure type).[13] The length of the Ge−Ge bonds within the zigzag chain is 2.492(2) Å, comparable with those in $(Eu_{1-x}Ca_x)_2Ge_2Pb$ and $EuLiGe_2$, but more than 0.1 Å shorter than d_{Ge-Ge} = 2.603(2) Å in EuGe.[13] This difference can be explained using the Zintl−Klemm concept.[5] If one were to rationalize the formula of EuGe, it would be $(Eu^{2+})(Ge^{2-})$, where each two-bonded Ge atom needs two extra electrons to satisfy the octet rule. This accounts for the formal charge of 2−, that is, 6 valence e^-/Ge-atom. Hence, in analogy with the electron count in the sulfur chains, for instance,[44] single bond order ought to be assigned to the Ge−Ge bonds in this compound. In $EuLiGe_2$, the structure is best rationalized as $(Eu^{2+})(Li^+)(Ge^{1.5-})_2$; that is, the possibility for partial double-bond order of the Ge−Ge bonds within the chains must be considered. This is done in analogy

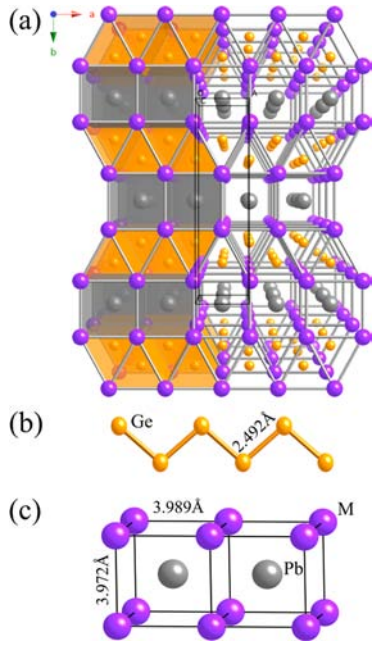

Figure 3. (a) Perspective view of the crystal structure of compound **II**. CsCl- and AlB_2-like fragments are emphasized. (b) The polyene-like [Ge_2] chains. (c) The 8-fold (distorted-cubic) coordination of the Pb atoms. Relevant interatomic distances are depicted.

with the polyacetylene chains, which are known to require between 5 and 6 e^-/atom.[44] The increase of the bond order can be correlated with the decrease of the bond distance (d_{Ge-Ge} = 2.4948(5) Å).

Applying the same electron counting arguments to compounds **I** and **II** is not a straightforward process because the role of the Pb atoms in the electronic structure is not easily understood from the analyses of the crystallographic data. Assuming no covalency of the Ge−Pb interactions (and neglecting the ionicity of the M−Pb ones; M = Eu/Ca or Eu/Sr), the formula of compound **II** could be broken down as $(M^{2+})_2(Ge^{2-})_2Pb$; however, this reasoning disagrees with the presumed polyene-like bonding in the [Ge_2] chains, implied from the relatively short (d_{Ge-Ge} = 2.492(2) Å) Ge−Ge bonds (Table 4). A different scheme would "borrow" the electron count from $EuLiGe_2$;[13] that is, each germanium atom will be assigned 5.5 valence e^-, and the overall count will be $(M^{2+})_2(Ge^{1.5-})_2Pb^{1-}$, which contradicts the very long M−Pb distances (>3.6 Å).

Table 4. Selected Interatomic Distances (in Å) in Compounds I and II

Compound I			
Ge1−Ge1	2.495(2)	M1−Ge1×2	3.125(1)
Ge1−Ge2	2.523(1)	M1−Ge2×2	3.126(1)
Pb1−Ge2	2.931(1)	M1−Ge2×2	3.244(1)
Pb1−Ge1	3.057(1)	M2−Ge1×2	3.209(1)
Pb1−Ge2	3.143(1)	M2−Ge2×2	3.264(1)
		M2−Ge1×2	3.388(1)
Compound II			
Ge1−Ge1×2		2.492(2)	
Pb1−Ge1×2		3.065(2)	
M1−Ge1×4		3.208(1)	
M1−Ge1×2		3.428(2)	

dx.doi.org/10.1021/ja3042838 | J. Am. Chem. Soc. 2012, 134, 12708−12716

Discerning the formal charges in compound **I** is even more complicated; after all, both compounds have the same nominal composition, but this structure features $[Ge_4]$ moieties, which have two terminal (1-bonded) germanium atoms (Figure 2). On the basis of the bond lengths in Figure 2, one could consider the molecular-like fragments as *trans*-butene-like $(Ge^{3-})-(Ge^{2-})=(Ge^{2-})-(Ge^{3-})$ species, but this formulation requires Pb to be treated as an electron donor, that is, $(M^{2+})_2(Ge^{3-})(Ge^{2-})_2Pb^{1+}$. With Pb being more electronegative than Ge,[42] this is clearly an implausible argument. Considering the $[Ge_4]$ unit as *trans*-1,3 butadiene, that is, $(Ge^{2-})=(Ge^{1-})-(Ge^{1-})=(Ge^{2-})$, alleviates the above problem but disagrees with the long–short–long bonding pattern of the Ge–Ge bonds (Figure 2). This brings us back to the idea of Ge–Pb covalency as the critical (and most unique) aspect of the chemical bonding in this instance.

3.2. Electronic Structure Calculations. To investigate the electronic structures for compounds **I** and **II** (Figure 4), first-principles calculations were carried out using plane-waves and pseudopotentials; complementary TB-LMTO calculations were carried out as well. Scalar relativistic effects were included, and the Eu atoms were found to adopt a $4f^76s^2$ electronic configuration when the Eu 4f electrons were treated explicitly as valence in the VASP calculations, agreeing with the Eu^{2+} state assigned experimentally (vide infra). Thus, in the results presented in the main text, the Eu 4f electrons were assigned to the core. Various ways to distribute the Eu/Ca or Eu/Sr atoms about the lattices were explored computationally. It was found that the manner in which the two sets of metals were distributed did not alter the densities of states (DOS) nor the ELF profile of the Pb/Ge layers substantially (see the Supporting Information). For the bonding analyses performed herein, the *Pbam*-$EuCaPbGe_2$ and *Amm*2-$EuSrPbGe_2$ structures, whose ELF profiles are illustrated in Figure 5, were employed as models for compounds **I** and **II**, respectively.

The projected densities of states (PDOS) obtained from the TB-LMTO calculations are given in Figure 4a. In general, the features agree well with the DOS obtained using pseudopotentials and plane-waves (the total DOS calculated via VASP for compound **I** is shown in the left panel of Figure 4b). The difference in the two sets of plots near the Fermi level stems from the fact that it was necessary to treat the Eu 5d electrons explicitly in the TB-LMTO calculations, whereas in VASP these were included in the pseudopotential.

Overall, the electronic structures of compounds **I** and **II** display numerous common characteristics. From −11 to −5 eV, the bands show primarily Pb and Ge s-character, with p-character dominating the valence set of the bands. There are minor contributions from the Eu and Ca/Sr atoms, mirroring similar observations in other intermetallic compounds.[45] Integrating the PDOS in the TB-LMTO calculations confirmed the Eu^{2+} state ($4f^7$ configuration). Interestingly, for both structures, a non-negligible amount of Ca and Sr d-orbital character was found below the Fermi level. It has been pointed out that in atoms, molecules, and solids containing Ca, Sr, and Ba, there is an increased amount of d-character in their bonds, and these can be considered as "honorary d-elements".[46] Back-donation into the d-orbitals, so that the metal does not assume a full 2+ oxidation state, has been observed.[47] Indeed, integrating the occupied d-states yields a charge of about 1+ for both Ca and Sr. Whereas this is suggestive of the configuration $(M^{1.5+})_2$ $(Ge^{1.5-})_2Pb^0$ for compound **II**, the

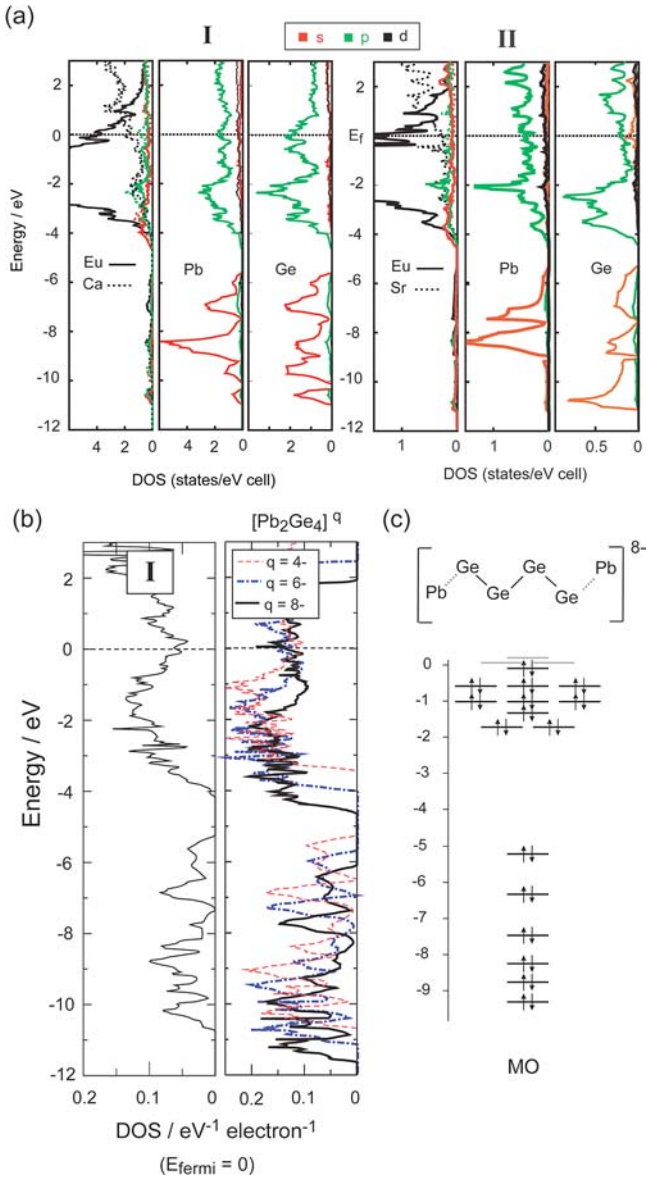

Figure 4. (a) Calculated site-projected densities of states of compounds **I** and **II** using TB-LMTO. (b) The total electronic densities of states of compound **I** and the electronic densities of states of its Pb/Ge sublattice with 8−, 6−, and 4− charges calculated using VASP. (c) A sketch of the molecular orbital level diagram of a Pb_2Ge_4 molecular fragment with a charge of 8−. The MO diagram and canonical MOs obtained for a charge of 4− were qualitatively similar. The Fermi energy and the HOMO energy are set to zero.

interactions in both systems, and in compound **I**, in particular, still require further analysis.

There are other indications that a full donation of the valence electrons from Eu and Ca/Sr to the Pb/Ge polyanions does not take place.[48] For both compounds, a hypothetical Pb/Ge substructure containing only one-half of the formal charge (assuming full ionization of the cations) reproduced the total DOS calculated using VASP well. This is illustrated in Figure 4b, wherein the DOS curves of negatively charged Pb/Ge sublattices extracted from compound **I** are compared to the total electronic DOS of the neutral system. The $[Pb_2Ge_4]^{8-}$ configuration represents the scenario where all of the valence electrons (assuming 2+ oxidation states for the Eu and Sr/Ca atoms) are donated into the Pb/Ge sublattice. The breadth of

dx.doi.org/10.1021/ja3042838 | J. Am. Chem. Soc. 2012, 134, 12708−12716

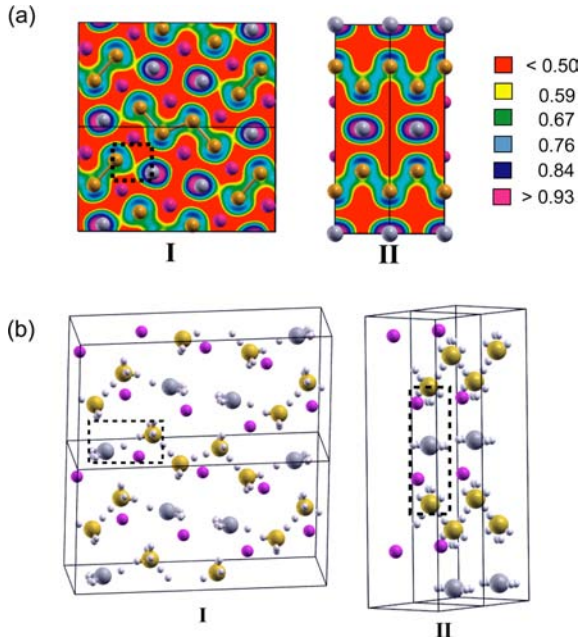

Figure 5. (a) Electron localization functions (ELF) of compounds **I** and **II**. (b) Bader maxima (shown as small white spheres) of the valence electron densities of compounds **I** and **II**, calculated using pseudopotentials and plane-waves.

the two sets of bands is never matched simultaneously (i.e., with the same charge); $q = 6-$ is needed to match up the valence set of bands, while $q = 4-$ is needed to match up the subvalence set of bands. The reason for the differences between the DOS curves of the real and hypothetical cases is not only due to the incomplete charge donation, but is also a result of the interplanar interactions of the cations with the Pb/Ge π-system in the neutral crystal; such interactions are noted in the literature.[49] This results in further dispersion of the valence set of bands, and, therefore, one could argue that the most representative electron count for compound **I** could be $[Pb_2Ge_4]^{4-}$. With this in mind, we looked for any subtle differences between the electronic structures of the two compounds.

The Electron localization function (ELF) values of compounds **I** and **II** calculated with VASP are shown in Figure 5a; plots obtained using TB-LMTO (provided in the Supporting Information) are very similar. Values representative of valence bonding[49] between Ge−Ge (near ELF = 0.75) can be pointed out; these are suggestive of four-membered Ge_4 molecular-like and infinite $[Ge_2]$ zigzag chains. The Ge and Pb lone pairs are signified by the regions with ELF > 0.8.

Similar computational results appeared in the literature while this Article was being finalized; Ge dimers and tetramers were found in the Ae_7Ge_6 structure (Ae = Ca, Sr, Ba), and Ge−Ge bonding was confirmed via Bader, ELF, and COHP analysis.[50] TB-LMTO yielded ELF values ranging from 0.59 to 0.63 between the Ge atoms in ref 50.

Importantly, we find a lower, but noninsignificant ELF of 0.59 between the Pb and Ge atoms in compound **I**. The corresponding ELF was calculated as being ∼0.70 in the $(p\text{-}Tol)_3PbGePh_3$ molecule;[29] however, Pb and Ge are the least electronegative heavy atoms in this structure, and therefore they assume positive partial charges, in stark contrast to what is found here. As a result of the very different oxidation states on the Ge and Pb atoms in $(p\text{-}Tol)_3PbGePh_3$ and the compounds studied in this work, the two will not be compared any further. The closeness of 0.59 to the ELF value representative of a homogeneous electron gas (0.5) initially caused us pause. However, we note that on moving down the periodic table localized orbitals become less localized, yielding lower ELF values, and metallic bonding also exhibits a diminished ELF.[51] To ensure the calculated value of 0.59 was particular to Pb−Ge bonding interactions and was not due to steric crowding, the ELF was calculated for compounds similar to **I**, but where the Pb atoms were substituted with Rn, Pt, Hg, Sn, and Ge (ignoring spin−orbit effects). The ∼0.6 ELF values were only maintained when Pb, Sn, or Ge was used (see the Supporting Information).

A topological feature of the ELF is the presence of reducible localization domains extending over the structure;[52] an f-localization domain contains the space enveloped by an iso-surface with iso-value f, and a reducible f-localization domain is one that will break into smaller localization domains at a higher iso-value. The 0.59-localization domain envelops Pb_2Ge_4 fragments, but there is no such domain >0.5 that envelops Pb and Ge atoms in compound **II**; see Figure 5a. At higher iso-values, the domain in compound **I** breaks into distinct domains encompassing Pb and Ge_4, and at 0.72 it further breaks into distinct lone-pair localization domains on each Pb and Ge atom. The 0.59 iso-value is comparable with the iso-values at saddle points between ELF attractors in several elemental metals (ranging from 0.525 to 0.635).[52] Also, the topological features of the ELF calculated using TB-LMTO for compound **I** were similar to those shown in Figure 5a, in the sense that there was a localization domain that encapsulates the Pb_2Ge_4 molecular fragment, but the highest isovalue needed to do so measures close to 0.50 instead of 0.59. It is interesting to note that the depleted ELF profile between Pb and Ge resembles a chemical system whose bonding has been described as neither covalent nor ionic, that of F_2.[53] We are not suggesting that Pb−Ge may also be described as a "charge-shift" bond,[54] but merely wish to emphasize the sparing use of the term "covalency" in this text.

Bader analysis of compounds **I** and **II** helped assign charges[55] of −0.51/−0.82/−1.00 to the Pb/Ge1/Ge2 atoms and −0.71/−0.74 to the Pb/Ge atoms, respectively. The volumes of the Bader basins ascribed to Pb are noticeably smaller in compound **I**, measuring 37.2 Å^3 versus 40.4 Å^3 for those in **II**, in line with the smaller negative charge computed and the increased steric crowding. In order to focus on the bonding, the Bader maxima for the valence electron density have been calculated; Figure 5b illustrates the local Bader maxima of electron density (shown as small white spheres) in the valence electron densities of compounds **I** and **II**. An apparent bonding interaction, outlined with a dashed-line rectangle, shows up as two maxima lined up between the Pb and Ge2 atoms in compound **I**, but not in compound **II**. The population of the basin along the Pb···Ge2 bond that lies closest to the Pb atom has roughly 11% of the charge density assigned to Pb (∼0.50 e), and the basin closest to the Ge2 atom has ∼4% (∼0.2 e) of the total valence charge density assigned to Ge2. For comparison, the Ge2 basin along the Ge2···Ge1 contact contains roughly 19% (∼0.9 e) of the charge density assigned to Ge2. Thus, both the ELF and the Bader analysis suggest a bonding interaction between Pb and Ge in compound **I**, which is weaker than the adjacent Ge2−Ge1 bond, but no such interaction in compound **II**.

Because the ELF and Bader analysis both indicate that the Pb_2Ge_4 molecular-like fragment is a viable building block of

dx.doi.org/10.1021/ja3042838 | J. Am. Chem. Soc. 2012, 134, 12708−12716

compound **I**, the electronic structure of "naked", that is, isolated, $[Pb_2Ge_4]^q$ molecular fragments with q = 8− and 4− was also considered. The energy spread (see Figure 4c) and symmetries of the canonical molecular orbitals (MOs) of these fragments were found to agree quite well with the presence of two sets of bands; the group of six MOs lowest in energy displayed predominantly Ge/Pb s-character, and the remaining occupied MOs higher in energy displayed primarily p-character. Upon optimization, the Ge2−Ge1, Ge1−Ge1, and Ge2−Pb distances in $[Pb_2Ge_4]^{4-}$ were found to be 2.53/2.50/2.68 Å (2.52/2.51/2.71 Å when spin−orbit coupling was included), in good agreement with those present in compound **I**. The computed Pb−Ge contact in the molecular fragment is somewhat shorter than the one observed in the solid, likely a result of interactions between Pb and Ge atoms on different chains, as discussed below.

TB-LMTO was used to calculate the crystal orbital Hamiltonian populations (COHPs)[32] of select interatomic contacts in both compounds **I** and **II**. At the top of Figure 6, we illustrate the qualitative link of the six canonical orbitals lowest in energy of a naked Pb_2Ge_4 fragment (whose MO level diagram is given in Figure 4c) with the COHP of the Pb−Ge2 contact in compound **I**. The bonding and antibonding interactions in the canonical MOs can explain the features in the COHP plot between −11 and −6 eV well. The second plot from the top shows the COHP between Pb and Ge atoms belonging to different fragments and suggests their interactions are far from negligible; in fact, the magnitude of the COHP around −11 eV is larger between the Pb and Ge atoms on different fragments. This is not unexpected, considering the second and third nearest neighbor Pb−Ge contacts are only 0.126 and 0.212 Å larger than the first.

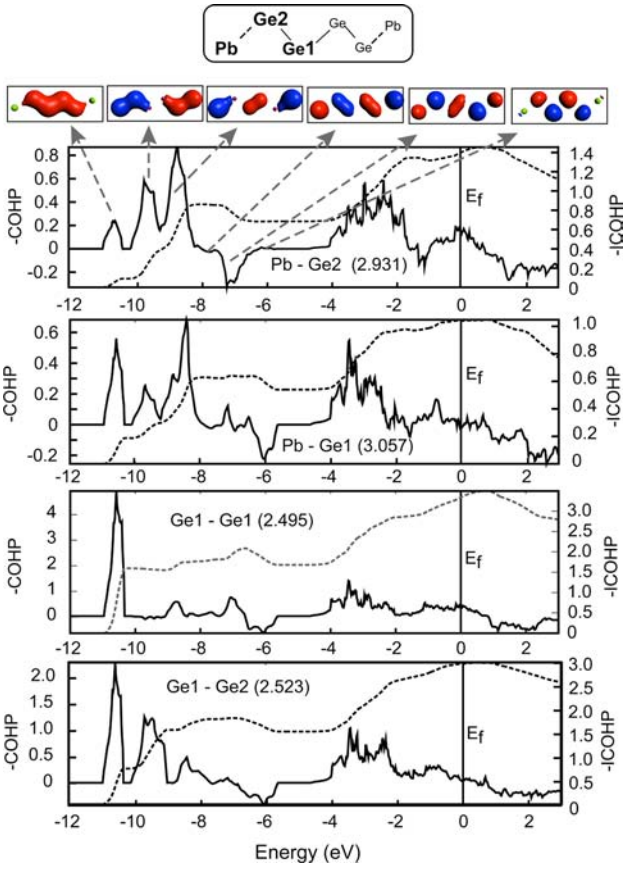

Figure 6. The calculated COHPs of various Pb/Ge contacts in compound **I** (shown as solid lines); the distance separating each atomic pair is given in angstroms and enclosed in braces. The integrated COHP (iCOHP) is traced by a dashed line and corresponds to the axis on the right of the plot. At the top of the figure, the qualitative agreement of the COHP of the Pb−Ge2 contact within a single fragment (measuring 2.931(1) Å) with the six lowest energy canonical orbitals of an isolated $[Pb_2Ge_4]^q$ molecule is shown. The units are bond^{-1} for the COHP plots and eV bond^{-1} mol^{-1} for the iCOHP.

The integrated COHP values (iCOHP) of select Ge/Pb contacts in both compounds **I** and **II** are shown in Table 5. It can be seen that the Ge−Ge iCOHPs all measure between 3.0 and 3.3, only slightly higher than the 2.42−2.81 range reported in the Ae_7Ge_6 structures.[50] The value between Pb and Ge2 in a single Pb_2Ge_4 fragment is roughly one-half that calculated for Ge−Ge, in agreement with the ELF and Bader charge analyses, which suggested that the charge density and electron localization function are weaker along the Pb−Ge2 contact. The iCOHPs between the next-nearest Ge and Pb atoms, which are 3.057 and 3.143 Å apart, are weaker, but only slightly, and roughly match with the Pb−Ge iCOHP calculated for compound **II**. The iCOHPs between Eu and Sr/Ca were always found to be <0.5. The calculated iCOHP values between the Pb/Ge sublattice and the Eu and Sr/Ca cations, however, are comparable with the Pb−Ge values; for the most part, they measure between 0.7 and 1.0. The largest such iCOHPs measure up to 1.2 and are between Ge and Ca.

Table 5. Select Distances (in Å) in Compounds I and II and Their Corresponding Crystal Orbital Hamiltonian Populations (iCOHPs) Integrated to the Fermi Energy

atom pair	distance [Å]	iCOHP [eV/bond mol]
	Compound **I**	
Ge1−Ge1	2.495	3.3
Ge2−Ge1	2.523	3.0
Pb−Ge2	2.931	1.4
Pb[a]−Ge1	3.057	1.0
Pb[a]−Ge2	3.143	0.9
Pb−Pb	3.829	0.2
Pb−Ca	3.502	0.6
Ge2−Ca	3.126	1.2
Ge1−Ca	3.125	1.1
	Compound **II**	
Ge−Ge	2.492	3.1
Pb−Ge	3.064	0.9
Pb−Pb	3.989	0.3
Pb−Sr	3.615	0.4
Ge−Sr	3.207	1.0

[a]These Pb and Ge atoms are from adjacent Pb_2Ge_4 fragments.

Finally, we show the energy bands of compound **II** (the simpler of the two structures) decorated by specified orbital characters in Figure 7. The Pb s-bands are full, and those containing character from p-orbitals, which are oriented both parallel and perpendicular to the zigzag germanium chains, cut the Fermi level. Thus, it appears reasonable to assume that Pb has a neutral oxidation state. As expected, three Ge sp^2-bands (σ-bands) and one pπ-band are completely full, and the remaining σ^* and pπ^*-bands are partially occupied. The band that is fourth lowest in energy displays substantial character

dx.doi.org/10.1021/ja3042838 | J. Am. Chem. Soc. 2012, 134, 12708−12716

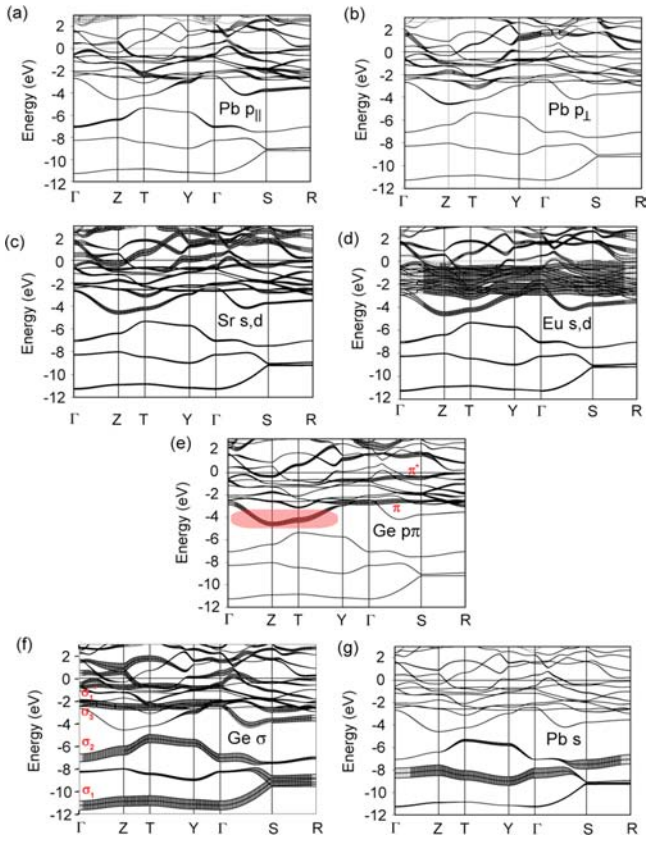

Figure 7. Energy bands for compound **II** decorated with orthonormal LMTO characters (fat bands). The Fermi energy is set as a reference level at zero energy. The highlighted red region in (e) displays Sr/Eu and Ge p−π character.

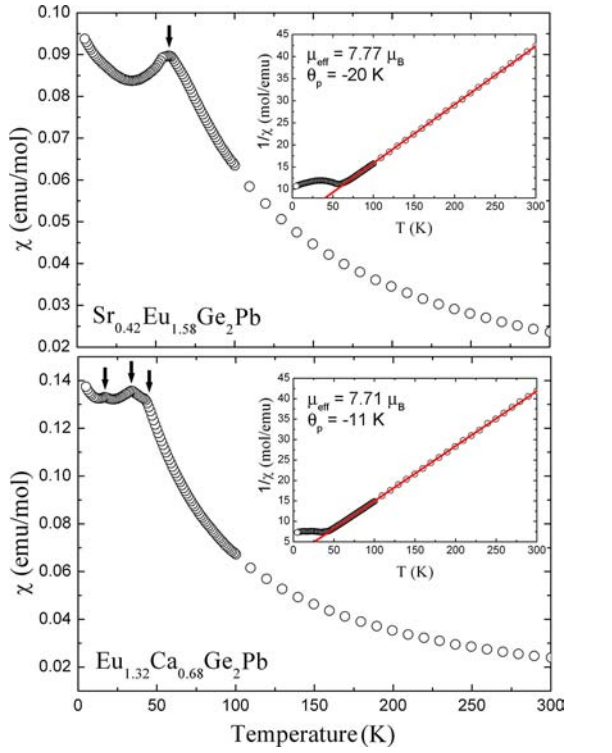

Figure 8. Temperature dependence of the DC-magnetic susceptibility of compounds **I** (bottom) and **II** (top). Insets: Inverse susceptibility versus temperature with linear fits to the Curie−Weiss law. The arrows indicate the Neel temperatures, below which the structures undergo antiferromagnetic ordering.

from both Sr and Eu atoms along Γ−Z−T−Y, as well as Ge-pπ; that is, the p-orbitals that lie perpendicular to the plane of the Ge-chains and point toward the layers containing Sr and Eu, indicative of an interplanar interaction between the cations and the Ge-chains.

The band structure of compound **I** (shown in Figure S11 in the Supporting Information) is more complicated than that of compound **II** because the unit cell contains 4 times as many atoms. The bands between −12 and −6 eV, as well as numerous bands between −4 eV and the Fermi level, exhibit both Pb σ/σ^* and Ge σ/σ^*-character. Above −4 eV, it is difficult to pick out distinct bands (both Ge/Pb σ/σ^* and π/π^*), due to their hybridization with Ca and Eu. Again, interplanar interactions between the cationic layers and those containing the Pb_2Ge_4 fragments are evident: around −5 to −4 eV a band exhibiting character from the Ge/Pb pπ as well as the Eu/Ca atoms along Γ−Z−T−Y is observed.

3.3. Magnetism. Plots of the molar magnetic susceptibilities ($\chi = M/H$) versus temperature are shown in Figure 8. In the high temperature regime, both compounds exhibit Curie−Weiss paramagnetism, as expected from the seven unpaired 4f electrons of Eu. The corresponding net effective moments and Weiss temperatures were derived by fitting the inverse of the susceptibility to a line, as show in the insets of Figure 8. The net effective moments of compounds **I** ($Eu_{1.32}Ca_{0.68(1)}Ge_2Pb$) and **II** ($Sr_{0.42}Eu_{1.58(2)}Ge_2Pb$) are 7.71 μ_B and 7.74 μ_B, respectively, which are very close to the expected value for free-ion Eu^{2+} ($S = 7/2$, $\mu_{eff} = 7.94\ \mu_B$) according to Hund's rule. This corroborates the existence of Eu in the divalent state. The negative Weiss temperatures suggest that both compounds undergo antiferromagnetic ordering at low temperatures. Indeed, below ca. 60 K, there is a cusp-like feature in the $\chi(T)$ curve of compound **II**, which is indicative of magnetic coupling with opposing spins. Similar magnetic response can also be found in other europium germanides such as EuGe (CrB type) and $EuLiGe_2$ ($CaLiGe_2$ structure type).[13] The mechanism for the observed antiferromagnetic ordering can be attributed to RKKY-type interactions. In compound **I**, there appear to be multiple magnetic ordering transitions below 60 K, suggesting more complex magnetic behavior. Likely, these successive transitions are due to the ordering of the two magnetic sublattices (recall there are two cation sites in compound **I**, but one in compound **II**), and more experimental work is needed to fully elucidate the nature of their magnetic responses.

4. CONCLUSIONS

The chemical bonding in $(Sr_xEu_{1-x})_2Ge_2Pb$ and especially in $(Eu_{1-x}Ca_x)_2Ge_2Pb$ is far from simple. Band structure and molecular calculations suggest that a full donation of electrons from the Eu and Ca/Sr to the Pb/Ge polyanionic sublattice does not take place. In the Sr-doped compound, this implies a neutral lead and a formal charge on Ge, which is indicative of partial double-bond character of the Ge−Ge bonds in the infinite [Ge_2] zigzag chains, in line with the relatively short Ge−Ge distances. Various analysis techniques have revealed that the Ca-doped compound, on the other hand, displays bonding between the Pb atoms and the *trans*-butene-like [Ge_4] units, which they cap. To this end, compound **I** represents the first realization of an ordered extended structure based on

dx.doi.org/10.1021/ja3042838 | J. Am. Chem. Soc. 2012, 134, 12708−12716

covalent Ge−Ge and Pb−Ge bonding. Current work to extend this chemistry to other systems is ongoing.

■ ASSOCIATED CONTENT

Supporting Information

Crystallographic information (in CIF format), additional structural information and discussion, computational results, and supporting electronic structure calculations. This material is available free of charge via the Internet at http://pubs.acs.org.

■ AUTHOR INFORMATION

Corresponding Author

bobev@udel.edu; ezurek@buffalo.edu

Notes

The authors declare no competing financial interest.

■ ACKNOWLEDGMENTS

S.B. acknowledges financial support from the National Science Foundation through grant DMR-0743916 (CAREER). E.Z. acknowledges the NSF (DMR-1005413) for financial support, and the CCR at SUNY Buffalo for computational support.

■ REFERENCES

(1) Schäfer, H.; Eisenmann, B. *Rev. Inorg. Chem.* **1981**, *3*, 29.
(2) Schäfer, H. *Annu. Rev. Mater. Sci.* **1985**, *15*, 1.
(3) Nesper, R. *Angew. Chem., Int. Ed. Engl.* **1991**, *30*, 789.
(4) Westbrook, J. H., Fleischer, R. L., Eds. *Intermetallic Compounds: Principle and Practice*; Wiley: New York, 1995.
(5) Kauzlarich, S. M., Ed. *Chemistry, Structure and Bonding of Zintl Phases and Ions*; VCH Publishers: New York, 1996, and the references therein.
(6) Guloy, A. M. Polar Intermetallics and Zintl Phases along the Zintl Border. *Inorganic Chemistry in Focus III*; Wiley-VCH Verlag GmbH & Co. KGaA: Weinheim, Germany, 2006.
(7) Corbett, J. D. *Inorg. Chem.* **2000**, *39*, 5178.
(8) DiSalvo, F. J. *Pure Appl. Chem.* **2000**, *72*, 1799.
(9) (a) Lupu, C.; Downie, C.; Guloy, A. M.; Albright, T. A.; Mao, J.-G. *J. Am. Chem. Soc.* **2004**, *126*, 4386. (b) Gout, D.; Benbow, E.; Gourdon, O.; Miller, G. J. *Inorg. Chem.* **2004**, *43*, 4604. (c) Björling, T.; Noréus, D.; Häussermann, U. *J. Am. Chem. Soc.* **2006**, *128*, 817. (d) Salvador, J. R.; Malliakas, C.; Gour, J. R.; Kanatzidis, M. G. *Chem. Mater.* **2005**, *17*, 1636. (e) Wang, L.; Tang, Z.; Lorenz, B.; Guloy, A. M. *J. Am. Chem. Soc.* **2008**, *130*, 11258.
(10) Corbett, J. D. *Inorg. Chem.* **2010**, *49*, 13.
(11) Suen, N.-T.; Tobash, P. H.; Bobev, S. *J. Solid State Chem.* **2011**, *184*, 2941.
(12) Guo, S.-P.; You, T.-S.; Bobev, S. *Inorg. Chem.* **2012**, *51*, 3119.
(13) Bobev, S.; You, T.-S.; Suen, N.-T.; Saha, S.; Greene, R.; Paglione, J.-P. *Inorg. Chem.* **2012**, *51*, 620.
(14) Tobash, P. H.; Bobev, S.; Thompson, J. D.; Sarrao, J. L. *J. Alloys Compd.* **2009**, *488*, 533.
(15) Bobev, S.; Bauer, E. D.; Thompson, J. D.; Sarrao, J. L.; Miller, G. J.; Eck, B.; Dronskowski, R. *J. Solid State Chem.* **2004**, *177*, 3545.
(16) The site preference problem in solids, also known as the "coloring" problem as coined by Prof. Gordon J. Miller (ref 17), requires a good estimation of the structural energy difference for different arrangement of atoms.
(17) Miller, G. J. *Eur. J. Inorg. Chem.* **1998**, 523.
(18) Kanatzidis, K. M.; Pöttgen, R.; Jeitschko, W. *Angew. Chem., Int. Ed.* **2005**, *44*, 6996.
(19) *Pearson's Handbook of Crystallographic Data for Intermetallic Phases*, 2nd ed.; Villars, P., Calvert, L. D., Eds.; American Society for Metals: Materials Park, OH, 1991.
(20) (a) *CRC Handbook of Chemistry and Physics*, 83rd ed.; CRC Press LLC: Boca Raton, FL, 2002. (b) Itkin, V. P.; Alcock, C. B. *J. Phase Equilib.* **1992**, *13*, 162.
(21) *SMART and SAINT*; Bruker AXS Inc.: Madison, WI, 2002.
(22) Sheldrick, G. M. *SADABS*; University of Göttingen: Germany, 2003.
(23) Sheldrick, G. M. *SHELXTL*; University of Göttingen: Germany, 2001.
(24) Gelato, L. M.; Parthe, E. *J. Appl. Crystallogr.* **1987**, *20*, 139.
(25) CIFs have all been deposited with Fachinformationszentrum Karlsruhe, 76344 Eggenstein-Leopoldshafen, Germany (fax, (49) 7247-808-666; e-mail, crysdata@fiz.karlsruhe.de) with depository numbers: CSD-424481 for $Eu_{1.32}Ca_{0.68(1)}Ge_2Pb$, and CSD-424482 for $Sr_{0.42}Eu_{1.58(2)}Ge_2Pb$.
(26) Kresse, G.; Hafner, J. *Phys. Rev. B* **1993**, *47*, 558.
(27) Blöchl, P. *Phys. Rev. B* **1994**, *50*, 17953.
(28) Perdew, J. P.; Burke, K.; Ernzerhof, M. *Phys. Rev. Lett.* **1996**, *77*, 3865.
(29) Koglin, H.-J.; Behrends, K.; Dräger, M. *Organometallics* **1994**, *13*, 2733.
(30) *ADF2012, SCM, Theoretical Chemistry*; Vrije Universiteit: Amsterdam, The Netherlands, http://www.scm.com.
(31) van Lenthe, E.; Baerends, E. J.; Snijders, J. G. *J. Chem. Phys.* **1993**, *99*, 4597.
(32) Dronskowski, R.; Blöchl, P. E. *J. Phys. Chem.* **1993**, *97*, 8617.
(33) Andersen, O. K. *Phys. Rev. B* **1975**, *12*, 3060.
(34) Andersen, O. K.; Jepsen, O. *Phys. Rev. Lett.* **1984**, *53*, 2571.
(35) Vosko, S. H.; Wilk, L.; Nusair, M. *Can. J. Phys.* **1980**, *58*, 1200.
(36) Perdew, J. P.; Wang, Y. *Phys. Rev. B* **1986**, *33*, 8800.
(37) Blöchl, P. E.; Jepsen, O.; Andersen, O. K. *Phys. Rev. B* **1994**, *49*, 16223.
(38) Formally, this is the Mo_2FeB_2 structure type, an ordered derivate of U_3Si_2 structure.
(39) The structure has the same space group and number of atoms in the unit cell as La_2Ni_2In (Pustovoychenko, M.; Svitlyk, V.; Kalychak, Ya. *Intermetallics* **2012**, *24*, 30), but the bonding patterns are subtly different because of the dissimilar *a*/*b* (0.506 vs 0.530), *a*/*c* (2.000 vs 1.733), and *b*/*c* (3.956 vs 3.273).
(40) Tobash, P. H.; Bobev, S. *J. Solid State Chem.* **2007**, *180*, 1575.
(41) Mao, J.-G.; Goodey, J.; Guloy, A. M. *Inorg. Chem.* **2002**, *41*, 931.
(42) Pauling, L. *The Nature of the Chemical Bond*; Cornell University Press: Ithaca, NY, 1960.
(43) Becher, H. J.; Krogmann, K.; Peisker, E. *Z. Anorg. Allg. Chem.* **1966**, *344*, 140.
(44) Papoian, G. A.; Hoffmann, R. *Angew. Chem., Int. Ed.* **2000**, *39*, 2408.
(45) For examples, see: (a) Whangbo, M.-H.; Lee, L.; Kohler, J. *Angew. Chem., Int. Ed.* **2006**, *45*, 7465. (b) You, T.-S.; Tobash, P. H.; Bobev, S. *Inorg. Chem.* **2010**, *49*, 1773.
(46) Pyykko, P. *J. Chem. Soc., Faraday Trans. 2* **1979**, *75*, 1256.
(47) Zurek, E.; Autschbach, J.; Malinowski, N.; Enders, A.; Kern, K. *ACS Nano* **2008**, *2*, 1000.
(48) Klem, M. T.; Vaughy, J. T.; Harp, J. G.; Corbett, J. D. *Inorg. Chem.* **2001**, *40*, 7020.
(49) Savin, A.; Nesper, R.; Wengert, S.; Fässler, T. F. *Angew. Chem., Int. Ed. Engl.* **1997**, *36*, 1808.
(50) Siggelkow, L.; Hlukhyy, V.; Fässler, T. F. *J. Solid State Chem.* **2012**, *191*, 76.
(51) See an early discussion of solid-state electronic structures: (a) Burdett, J. K. *J. Phys. Chem. A* **1996**, *100*, 13263. or the first reports of ELF plots applied to solid-state structures: (b) Savin, A.; Jepsen, O.; Flad, J.; Andersen, O. K.; Preuss, H.; von Schnering, H.-G. *Angew. Chem., Int. Ed. Engl.* **1992**, *31*, 187.
(52) Silvi, B.; Gatti, C. *J. Phys. Chem. A* **2000**, *104*, 947.
(53) (a) Shaik, S.; Danovich, D.; Silvi, B.; Lauvergnat, D. L.; Hiberty, P. C. *Chem.-Eur. J.* **2005**, *11*, 6358. (b) Llusar, R.; Beltran, A.; Andres, J.; Noury, S.; Silvi, B. *J. Comput. Chem.* **1999**, *20*, 1517.
(54) Shaik, S.; Danovich, D.; Wu, W.; Hiberty, P. C. *Nat. Chem.* **2009**, *1*, 443.
(55) Tang, W.; Sanville, E.; Henkelman, G. *J. Phys.: Condens. Matter* **2009**, *21*, 084204.